

Linköping University Post Print

Structural anisotropy of nonpolar and semipolar InN epitaxial layers

Vanya Darakchieva, Mengyao Xie, N Franco, F Giuliani, B Nunes, E Alves, C L Hsiao, L C Chen, T Yamaguchi, Y Takagi, K Kawashima and Y Nanishi

N.B.: When citing this work, cite the original article.

Original Publication:

Vanya Darakchieva, Mengyao Xie, N Franco, F Giuliani, B Nunes, E Alves, C L Hsiao, L C Chen, T Yamaguchi, Y Takagi, K Kawashima and Y Nanishi, Structural anisotropy of nonpolar and semipolar InN epitaxial layers, 2010, JOURNAL OF APPLIED PHYSICS, (108), 7, .

<http://dx.doi.org/10.1063/1.3487923>

Copyright: American Institute of Physics

<http://www.aip.org/>

Postprint available at: Linköping University Electronic Press

<http://urn.kb.se/resolve?urn=urn:nbn:se:liu:diva-61185>

Structural anisotropy of nonpolar and semipolar InN epitaxial layers

V. Darakchieva,^{1,2,a)} M.-Y. Xie,^{1,2} N. Franco,¹ F. Giuliani,³ B. Nunes,⁴ E. Alves,¹ C. L. Hsiao,⁵ L. C. Chen,⁵ T. Yamaguchi,⁶ Y. Takagi,⁶ K. Kawashima,⁶ and Y. Nanishi⁶

¹Instituto Tecnológico e Nuclear, 2686-953 Sacavém, Portugal

²Department of Physics, Chemistry, and Biology, Linköping University, SE-581 83 Linköping, Sweden

³Department of Materials, Center for Advanced Structural Ceramics, Imperial College, 2W7 2AY London, United Kingdom

⁴Dep. de Engenharia de Materiais, Instituto Superior Técnico, 1049-001 Lisboa, Portugal

⁵Center for Condensed Matter Sciences, National Taiwan University, Taipei 106, Taiwan

⁶Department of Photonics, Ritsumeikan University, Shiga 525-8577, Japan

(Received 31 May 2010; accepted 28 July 2010; published online 13 October 2010)

We present a detailed study of the structural characteristics of molecular beam epitaxy grown nonpolar InN films with *a*- and *m*-plane surface orientations on *r*-plane sapphire and (100) γ -LiAlO₂, respectively, and semipolar (10 $\bar{1}$ 1) InN grown on *r*-plane sapphire. The on-axis rocking curve (RC) widths were found to exhibit anisotropic dependence on the azimuth angle with minima at InN [0001] for the *a*-plane films, and maxima at InN [0001] for the *m*-plane and semipolar films. The different contributions to the RC broadening are analyzed and discussed. The finite size of the crystallites and extended defects are suggested to be the dominant factors determining the RC anisotropy in *a*-plane InN, while surface roughness and curvature could not play a major role. Furthermore, strategy to reduce the anisotropy and magnitude of the tilt and minimize defect densities in *a*-plane InN films is suggested. In contrast to the nonpolar films, the semipolar InN was found to contain two domains nucleating on zinc-blende InN(111)A and InN(111)B faces. These two wurtzite domains develop with different growth rates, which was suggested to be a consequence of their different polarity. Both, *a*- and *m*-plane InN films have basal stacking fault densities similar or even lower compared to nonpolar InN grown on free-standing GaN substrates, indicating good prospects of heteroepitaxy on foreign substrates for the growth of InN-based devices. © 2010 American Institute of Physics. [doi:10.1063/1.3487923]

I. INTRODUCTION

Group-III nitrides have revolutionized solid state lighting by enabling light emitting diodes from the deep ultraviolet to amber and laser diodes in the violet and blue, and have led to significant advances in high power/high frequency electronics. Recently, nitride materials with nonpolar/semipolar surface orientations (i.e., with the *c*-axis parallel/inclined to the growth plane) have attracted considerable attention due to the possibility to avoid/minimize the built-in electric fields in nonpolar/semipolar nitride heterostructures.^{1,2}

Nonpolar nitride films with *a*-plane and *m*-plane orientations (see Fig. 1) have been grown on *r*-plane sapphire,³ (100) γ -LiAlO₂,¹ *a*- and *m*-plane SiC,^{4,5} and more recently on *a*- and *m*-plane GaN substrates.^{6,7} Semipolar nitride films have been mostly grown by using lateral epitaxial overgrowth techniques⁸ but also on *m*-plane sapphire,⁹ Si(001),¹⁰ and semipolar GaN bulk substrates.^{11,12}

The structural characteristics of the nonpolar and semipolar nitride films are expected to be anisotropic as a result of the anisotropies of film and substrate surfaces. Indeed, the full widths at half maximum (FWHMs) of the on-axis (11 $\bar{2}$ 0) rocking curves (RCs) of *a*-plane GaN films were reported to have either an “M” or a “W” shape dependence on the azi-

muth angle with minimum FWHM parallel to the GaN [0001] or [1 $\bar{1}$ 00] directions.^{13–16} Similar azimuth dependence of the on-axis (1 $\bar{1}$ 00) RC FWHM has also been reported for *m*-plane GaN films.¹⁷ The anisotropic behavior of the RC FWHM in nonpolar GaN films was attributed to the combined or sole effect of anisotropic distribution of dislocations,^{14,15} tilt,¹⁵ wafer bending,¹⁶ and stacking faults.^{17,18} Surface roughness was also shown to affect the RC broadening¹⁸ and therefore may further contribute to the

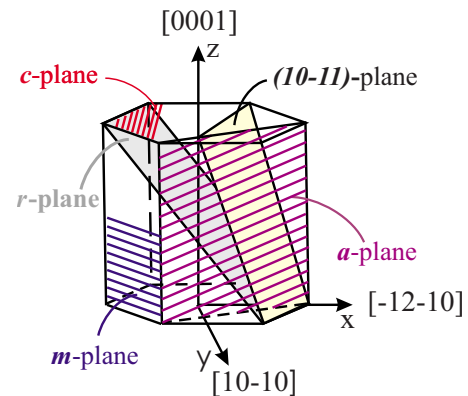


FIG. 1. (Color online) Schematic presentation of the wurtzite crystal structure of group-III nitrides. Hatched areas indicate the most often used planes for epitaxial growth: the polar *c*-plane (0001); the nonpolar *a*-plane (11 $\bar{2}$ 0) and *m*-plane (1 $\bar{1}$ 00); and the semipolar *r*-plane (1 $\bar{1}$ 02) and (10 $\bar{1}$ 1).

^{a)}Electronic mail: vanya@ifm.liu.se.

TABLE I. Summary of growth conditions and thickness of the nonpolar and semipolar InN films: thickness, d , nitridation temperature, T_{nitr} , nitridation time, t_{nitr} , buffer layer growth temperature, T_{buff} , and growth temperature of the main layer, T_{gr} .

Sample	d (nm)	T_{nitr} (°C)	t_{nitr} (min)	T_{buff} (°C)	T_{gr} (°C)
(11 $\bar{2}$ 0): A1	695	200	120	...	420
(11 $\bar{2}$ 0): A2	513	250	120	...	400
(11 $\bar{2}$ 0): A3	500	RT	120	350	450
(1 $\bar{1}$ 00)	400	450
(10 $\bar{1}$ 1)	370	420

observed anisotropy.¹⁹ Reports on the structural anisotropy of semipolar GaN just begun to emerge and the on-axis RC of semipolar (11 $\bar{2}$ 2) GaN films have been recently found to also exhibit anisotropic behavior.²⁰

The structural anisotropy of nonpolar III-nitride films affects their optical performance and device-relevant characteristics (carrier mobility, degradation, etc.), which requires detailed study of these issues. While the structural anisotropy of nonpolar GaN films have been extensively studied^{1,14–17,21–23} the information on the structural characteristics of nonpolar InN is very scarce^{24,25} and detailed reports exists only for films grown on GaN substrates.^{26,27} However, the nonpolar GaN substrates are not only extremely expensive but also have a limited supply. The heteroepitaxy on foreign substrates is still the practical way to get large scale InN and related alloys and device heterostructures at low cost. Furthermore, nothing is known for the case of semipolar InN.

In this work, we report a study of the structural anisotropy of heteroepitaxial a -plane and (10 $\bar{1}$ 1) oriented InN films grown on (1 $\bar{1}$ 02) sapphire and m -plane InN film grown on (100) γ -LiAlO₂ substrates, respectively. The mosaic anisotropy in the nonpolar and semipolar InN films is obtained and discussed in terms of rotational disorder (tilt) and defects.

II. EXPERIMENTAL

Nonpolar and semipolar InN films with thicknesses of about 370–700 nm were grown by molecular beam epitaxy (MBE). The a -plane films were grown on (11 $\bar{2}$ 0) (r -plane) sapphire substrates employing nitridation pretreatment of the substrates^{28,29} or low-temperature (LT) InN buffer layer.³⁰ The (10 $\bar{1}$ 1)-oriented and the m -plane InN films were grown directly on (1 $\bar{1}$ 02) sapphire²⁸ and (100) γ -LiAlO₂,³⁰ respec-

tively. A summary of the growth conditions and film thicknesses is given in Table I. The growth temperatures are chosen to be below the dissociation temperature,²⁷ which is much lower than the respective dissociation temperature for N-polar c -plane InN and comparable to the case of In-polar c -plane InN.³⁰ All films show n -type conductivity and rather smooth surface morphology with root-mean-square (rms) roughness below 11 nm. The bulk free electron concentrations in the a -plane films range from 4×10^{18} to 1×10^{19} cm⁻³ with good electron mobilities reaching 370 cm²/V s,³¹ being superior to the mobilities previously reported for a -plane InN films with comparable thicknesses.^{24,32} The (10 $\bar{1}$ 1)- and the m -plane films exhibit bulk free electron concentrations in the low 10^{18} cm⁻³ and mid 10^{19} cm⁻³ range, and electron mobilities of 270 cm²/V s and 200 cm²/V s, respectively. Further details about the growth procedure, nucleation schemes, and film properties can be found in Refs. 28–31.

X-ray diffraction (XRD) RC, reciprocal space map (RSM), and pole figure (PF) measurements were performed using monochromated Cu $K\alpha_1$ radiation on a D8Discover system from Bruker-AXS. A Göbel mirror and an asymmetric 2-bounce Ge(220) monochromator were used on the primary side and a scintillation detector was employed on the secondary side. The RCs and PFs were acquired with an open detector without slits or analyzer in the secondary beam while the RSMs and radial scans were recorded with 0.1 mm slit in front of the detector. A Veeco DI CP-II atomic force microscope was used for the topographic characterization. Silicon etched probes, with a nominal radius of 10 nm and a nominal constant of 40 N/m, were used. The imaging was performed in noncontact dynamic mode, at room humidity and temperature conditions. The rms roughness of the samples was measured on 5×5 μm^2 areas. Transmission electron microscopy (TEM) specimens were prepared by focused ion beam milling using a Zeiss 1540 EsB cross beam instrument following the lift out technique. The cross-sectional TEM images were obtained in a FEI Tecnai G2 ultratwin microscope operating at 200 KV.

III. RESULTS AND DISCUSSION

Figure 2 shows atomic force microscopy (AFM) images of the a -plane, m -plane, and (10 $\bar{1}$ 1)-oriented InN films. The a -plane InN films exhibit grainy surface structure indicative of three-dimensional (3D) growth mode and the rms surface roughness varies between 3.9 and 10.5 nm depending on the growth and nucleation conditions (Table I). These values are well within the range of rms surface roughness reported for

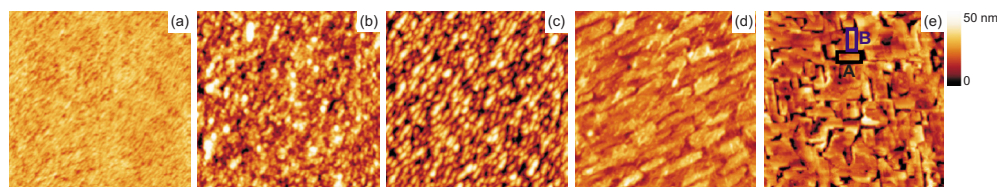


FIG. 2. (Color online) 5×5 μm^2 AFM images of the a -plane InN: (a) film A1, (b) film A2, (c) film A3, (d) the m -plane InN film, and (e) the semipolar (10 $\bar{1}$ 1) InN film. The two domains, A and B, rotated with respect to each other by $\sim 90^\circ$ are indicated in (e).

a-plane InN grown on *r*-plane sapphire using GaN buffer layers.²⁴ Similar surface morphologies were previously reported for *a*-plane InN films grown by MBE on *r*-plane sapphire²⁴ and free-standing GaN substrates.²⁷ We note that the observed surface morphology differs from the typical striated surface morphology (with striations along the [0001] direction) of *a*-plane GaN films, often decorated with surface pits.^{3,13,18,19,33} The *m*-plane InN film exhibits a periodic trenchlike surface structure and a surface roughness of 6.9 nm. This trenchlike surface morphology most likely replicates the surface morphology of the substrate, as previously shown for *m*-plane GaN films grown on LiAlO₂.³⁴ The surface morphology of the semipolar film reveals two rectangular domains rotated with respect to each other by approximately 90° [Fig. 2(e)]. This is in contrast to the isotropic surface morphologies of the nonpolar films. The apparent anisotropy of the surface morphology of the semipolar film could be related to its structural anisotropy, which is more complicated compared to the nonpolar case (see Sec. III B 3).

3D nucleation, coalescence, and growth were also recently reported for *a*-plane InN grown on *r*-plane sapphire using GaN buffer layers,²⁴ and which is in contrast with the two-dimensional growth typical for polar InN. The 3D growth of our non(semi)polar InN may be related to the fact that the heteroepitaxy of these films was performed on non-isostructural foreign substrates, which have different surface atomic arrangements than those of the non(semi)polar InN films. The lattice mismatches between films and substrates along the two main crystallographic in-plane directions are different. For instance, lattice mismatches between *m*-plane InN and LiAlO₂ along [12 $\bar{1}$ 0]InN||[001]LiAlO₂ and [0001]InN||[010]LiAlO₂ are 13% and 10%, respectively.²⁵ The growth mode of *a*-plane InN may be further affected by the relatively low growth temperature and a possible presence of misoriented crystallites promoted by the nitridation of the substrate.³⁵

A. Assessment of film structure by XRD

Within the mosaic block model the broadening of the on-axis symmetric RC is affected by the coherence lengths of the crystallites in lateral direction (parallel to the sample surface) and their tilt. These sources of broadening have different functional dependencies on the scattering order, which can be used to separate the two contributions to the RC broadening by the Williamson–Hall plot.^{36,37} The Williamson–Hall plot is a plot of the RC width, FWHM $\times (\sin \theta)/\lambda$, as a function of the reflection order, $(\sin \theta)/\lambda$, where θ and λ are the angle of incidence and the wavelength of the x-rays. The tilt is then obtained from the slope of the linear dependence and the lateral coherence length (LCL) is derived from the inverse of the intersection with the ordinate.^{36,37}

The LCL of the mosaic blocks is affected by the density of planar and extended defects. Basal plane stacking faults (BPSFs) are among the most abundant defects in nonpolar nitride films, in particular the intrinsic I_1 -type BPSFs.^{15,17,18,33} However, the two accessible on-axis reflec-

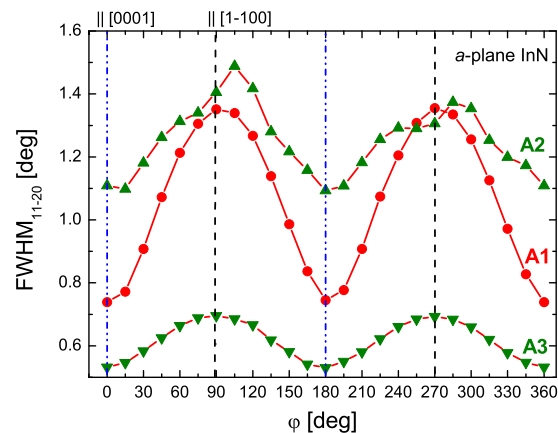


FIG. 3. (Color online) FWHM of the on-axis (11 $\bar{2}$ 0) RC for the *a*-plane InN films.

tions for *a*-plane InN, i.e., (11 $\bar{2}$ 0) and (22 $\bar{4}$ 0), are unaffected by the BPSF.^{18,27} Therefore, the respective Williamson–Hall plots would give LCLs that are greatly overestimated. Nevertheless, these LCLs could be instructive for the distribution of defects different from BPSFs or other structural characteristics.

The presence of BPSFs affects the (1 $\bar{1}$ 00) and (2 $\bar{2}$ 00) RC broadening in [0001] direction for *a*-plane, *m*-plane, and semipolar films (the broadening in perpendicular direction is not affected by BPSFs), while the (3 $\bar{3}$ 00) RC is insensitive.^{18,27} Therefore, LCLs sensitive to the BPSF density, could be derived from the Williamson–Hall plot analysis of the ($h\bar{h}00$) reflections ($h=1,2$). The BPSF density can be then estimated on the assumption that BPSF are the main factor determining the limited LCLs. This method was used to estimate the BPSFs in *m*-plane GaN (Ref. 17) and *a*-plane²⁶ and *m*-plane InN (Ref. 27) films grown on bulk GaN. In all these cases good agreement between the BPSF densities determined from XRD and TEM was found. We followed the same approach and measured the ($h\bar{h}00$) RCs in skew symmetric geometry for the *a*- and semipolar InN films, and in normal symmetric geometry for the *m*-plane InN film. In the case of *a*-plane InN this was only possible for azimuth positions parallel to the InN [0001] while for the semipolar film—only for azimuth perpendicular to the InN [0001] due to the inaccessibility of the reflections for the respective orthogonal directions.

Figures 3, 7, and 12 show the RC FWHMs of the on-axis (11 $\bar{2}$ 0), (1 $\bar{1}$ 00), and (10 $\bar{1}$ 1) reflections as a function of the azimuth orientation of the diffraction plane with respect to the InN [0001] direction for our *a*-plane, *m*-plane, and semipolar InN films, respectively. We performed the on-axis ($h\bar{h}2\bar{h}0$) and ($h\bar{h}00$) Williamson–Hall plot analyzes for the *a*- and *m*-plane InN films, respectively, at all azimuth positions and selected results for the two orthogonal in-plane directions are presented in Figs. 4 and 9. The azimuth dependencies of the derived tilt and LCLs are presented in Figs. 5 and 8. In addition, the (1 $\bar{1}$ 00) WHP analyzes were also performed for the *a*-plane and semipolar InN films at azimuth position parallel and perpendicular to the InN [0001], respec-

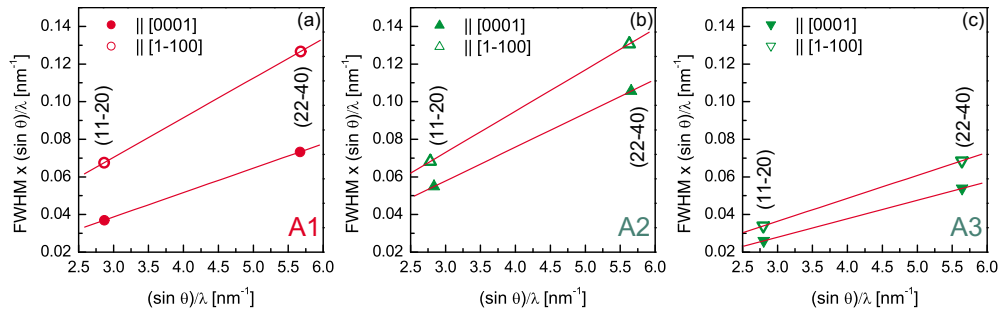


FIG. 4. (Color online) Williamson–Hall plots of the on-axis ($hh\bar{2}h0$) RCs for the a -plane InN films at azimuth positions parallel and perpendicular to the InN [0001]: (a) film A1, (b) film A2, and (c) film A3.

tively (Figs. 6 and 13). The FWHMs of the $(11\bar{2}0)$, $(10\bar{1}1)$, and $(1\bar{1}00)$ RCs, the values of the tilt, LCLs, and the BPSF densities for the two orthogonal in-plane directions are listed in Table II together with the rms roughness for the a -plane, m -plane, and semipolar InN films. The $(10\bar{1}1)$ PF and a cross-section high-resolution TEM (HRTEM) image taken at the interface of the semipolar InN film are shown in Figs. 10 and 11, respectively.

B. Structural anisotropy

1. a -plane InN

The on-axis RC FWHMs of all a -plane InN films show minima at azimuth positions parallel to the InN [0001] direction and maxima for the perpendicular direction (Fig. 3). The degree and magnitude of the RC anisotropy depend on the sample. Such an “M”-shape anisotropic behavior of the RC width was previously reported for relatively thin a -plane GaN films grown by hydride vapor phase epitaxy (HVPE) (Ref. 16) and by metalorganic vapor phase epitaxy (MOVPE) using a ScN buffer layer,¹⁸ for example. On the other hand, a -plane InN films grown on free-standing GaN substrates show slightly higher $(11\bar{2}0)$ RC broadenings along the InN [0001] direction compared to the respective values for $[1\bar{1}00]$.²⁷ We note that the RC FWHMs of our a -plane InN film grown with a LT buffer layer (film A3, see Table II)

are comparable with the respective values reported for an a -plane InN film grown under optimal conditions (the lowest BPSF density) on GaN substrate.²⁷ The latter being 0.56° and 0.49° for the [0001] and $[1\bar{1}00]$, respectively. However, the RC anisotropy in our InN film A3 is still slightly larger than the one reported for the a -plane InN film grown on GaN substrate.²⁷

The HRXRD RSMs around the InN 213 reciprocal space point (not shown here) of our a -plane InN films exhibited elliptical broadening typical for group-III nitride heteroepitaxial films.³⁸ We found that the inclination angles of the main axes of these ellipses with respect to the lateral scattering vector are very close to the angle between the diffracting plane and the surface for all films. This is a strong indication that the dominant broadening of the reciprocal lattice points is due to the mosaic tilt.³⁷ This is further confirmed by the $(hh\bar{2}h0)$ Williamson–Hall plots analyzes (Fig. 4) revealing large tilts in the films that correlate with the observed RC anisotropy (see Table II and Figs. 3 and 5).

A comparison between our a -plane InN films grown without a buffer layer (A1 and A2) shows that a lower anisotropy of the tilt is observed for the film A2 grown using a higher nitridation temperature (Fig. 5 and Table I). On the other hand, the magnitude of the rotational disorder is lower in the film A1 grown at higher growth temperature. The structure, orientation and crystallinity of the nucleation centers formed during the substrate nitridation will govern the growth habit of the subsequent InN crystallites. Therefore, a

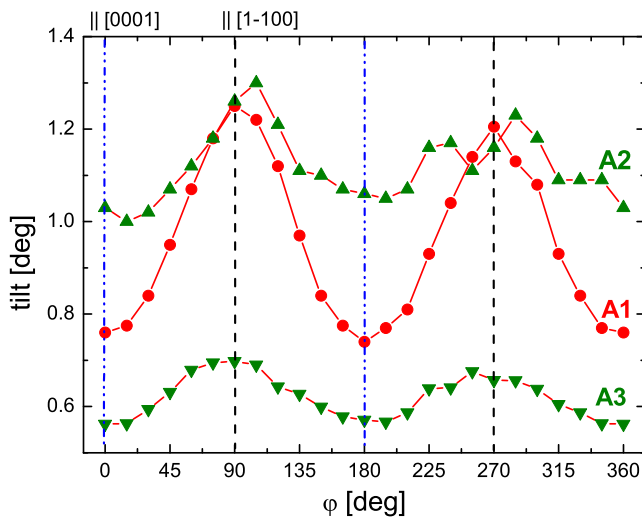


FIG. 5. (Color online) Azimuth dependence of the tilt for the a -plane InN films.

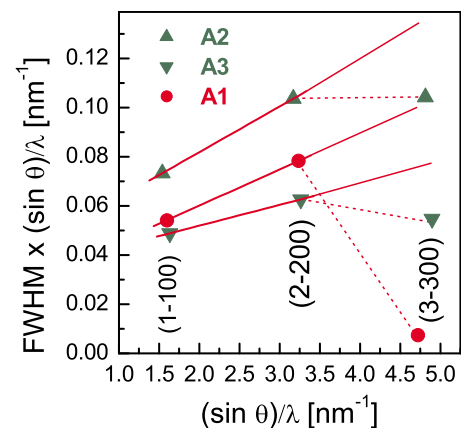


FIG. 6. (Color online) Williamson–Hall plots of the $(h\bar{h}00)$ RCs for the a -plane InN films at azimuth positions parallel to the InN [0001].

TABLE II. Summary of structural parameters of the nonpolar and semipolar InN films for the two orthogonal in-plane directions parallel and perpendicular to the InN [0001]: FMHW of the (11 $\bar{2}$ 0) or (10 $\bar{1}$ 1) RCs for the *a*-plane and semipolar films, respectively, $\Delta\omega(11\bar{2}0)/(10\bar{1}1)$; FMHW of the (1 $\bar{1}$ 00) RC, $\Delta\omega(1\bar{1}00)$; tilt, α ; LCLs determined from the (*hh*2 \bar{h} 0) Williamson–Hall plots for the *a*-plane films (Fig. 3) or the (*h*0 $\bar{h}h$) Williamson–Hall plots for the semipolar InN, LCL^{(*hh*2 \bar{h} 0)/(*h*0 $\bar{h}h$)}; LCL determined from the (*h* \bar{h} 00)_{*h*=1,2} Williamson–Hall plots (Fig. 5), LCL^(*h* \bar{h} 00); BPSF density, ρ_{SF} ; and rms surface roughness measured from 5 × 5 μm^2 atomic force microscopy scans, SR.

Sample	$\Delta\omega(11\bar{2}0)/(10\bar{1}1)$ (deg)		$\Delta\omega(1\bar{1}00)$ (deg)		α (deg)		LCL ^{(<i>hh</i>2\bar{h}0)/(<i>h</i>0$\bar{h}h$)} (nm)		LCL ^(<i>h</i>\bar{h}00) (nm)		ρ_{SF} (10 ⁵ cm ⁻¹)	SR (nm)
	[0001]	\perp [0001]	[0001]	\perp [0001]	[0001]	\perp [0001]	[0001]	\perp [0001]	[0001]	\perp [0001]		
(11 $\bar{2}$ 0): A1	0.74	1.35	1.94	...	0.76	1.25	>5000	62	15	...	6.8	3.9
(11 $\bar{2}$ 0): A2	1.11	1.41	2.73	...	1.03	1.26	291	63	10	...	9.9	7.6
(11 $\bar{2}$ 0): A3	0.53	0.70	1.71	...	0.56	0.70	>5000	25	13	...	7.8	10.5
(1 $\bar{1}$ 00)	1.82	0.64	0.33	0.68	11	319	9.2	6.9
(10 $\bar{1}$ 1)A	1.99	0.98	...	0.97	1.7	3.16	201	131	...	6.6
(10 $\bar{1}$ 1)B	2.07	1.03	...	0.95	0.61	2.21	12	592	...	6.6

lower spread of the rotational disorder may be expected when the nitridation is performed at higher temperature enabling improved crystallinity. In this respect we also point out that an interface layer of single-crystalline zinc-blende AlN was found to form in the case of the A2 film,²⁹ while an amorphous AlO_xN_y was formed at the interface when the nitridation is performed at lower temperature, such as for film A1.²⁸ The growth temperature, on the other hand, will affect the adatom mobility during the growth of the InN film and will promote an improved film crystal quality. Our observations suggest that a higher nitridation temperature or an optimized nucleation scheme combined with a higher growth temperature may enable both lower anisotropy and magnitude of the rotational disorder. This is confirmed by the results for film A3 grown with a LT buffer layer (350 °C) and at a higher growth temperature compared to films A1 and A2 (Tables I and II). Both the anisotropy and the magnitude of the tilt are substantially reduced for film A3.

The (*hh*2 \bar{h} 0) Williamson–Hall plot analyzes of our *a*-plane films (Fig. 4) further revealed well pronounced anisotropy of the LCLs with the azimuth angle with maxima for the InN [0001] direction and minima for the perpendicular direction (Table II). The LCLs in the [0001] directions for films A1 and A3 grown at higher growth temperatures (Table I) exceed the evaluation limit of 5 μm . The as extracted LCLs are not affected by the presence of BPSFs due to the insensitivity of the (*hh*2 \bar{h} 0) reflections to BPSFs.^{18,27} Therefore, the observed anisotropy of the LCLs should be related to other structural characteristics such as different film curvatures or geometrical sizes of the crystallites along the two orthogonal in-plane directions, specific distribution of dislocations, etc.

Recently, the surface roughness was suggested to affect the anisotropic (11 $\bar{2}$ 0) RC broadening in MOVPE *a*-plane GaN films¹⁹ showing the typical surface striation morphology.³³ The authors reported greater surface-related RC broadening for direction perpendicular to the GaN [0001] with increasing surface roughness while a maximum RC broadening in [0001] is observed for the smoother film.¹⁹ In contrast to these results, the RC FWHMs of our smooth *a*-plane InN films (our *a*-plane InN films are significantly

smoother than the *a*-plane GaN from Ref. 19 with RMS roughness of 80 nm and 32 nm) show minima for direction parallel to the InN [0001]. Furthermore, we do not find any increase in the RC broadening in [1 $\bar{1}$ 00] direction with increasing surface roughness of the *a*-plane InN films (Table II and Fig. 3). These observations suggest that the surface roughness does not play a major role for the anisotropic behavior of the (11 $\bar{2}$ 0) RCs and associated LCLs in our *a*-plane InN films.

Generally, the bending of nitride films thinner than 1 μm should be relatively small for the thickness of the sapphire substrate used,³⁹ and it is not expected to affect significantly the on-axis RC broadening. Indeed, anisotropic curvatures have been reported for HVPE *a*-plane GaN films and suggested to be the dominant contribution to the RC broadening only for films thicker than 20 μm .^{15,16} On the other hand, the curvature of MOVPE *a*-plane GaN films was reported to be practically independent on the rotation.¹⁸ In order to evaluate the effect of the curvature on the anisotropic behavior of the (11 $\bar{2}$ 0) RC FWHM in our films we performed RC measurements with different beam sizes for each of the two orthogonal in-plane directions. The restriction of the beam size leads to slight narrowing (1% to 5%) of the RCs indicating that the contribution from the film bending to the RC broadening is very small. The RC narrowing is more noticeable for the azimuth position parallel to the InN [0001] for films A1 and A2 while the opposite trend is observed for film A3. Film A3, exhibiting the most pronounced difference in the (11 $\bar{2}$ 0) LCLs (Table II), does not show a significant anisotropy of the RC narrowing upon beam restriction. This indicates that although film bending may contribute to the RC broadening, it is unlikely to be the main factor causing the observed large difference in the LCLs for our *a*-plane InN films. On the other hand the geometrical size of the mosaic blocks may be the limiting factor for the LCLs. In such case a higher growth rate of the crystallites in the InN [0001] direction compared to the [1 $\bar{1}$ 00] may explain the observed anisotropy in the LCLs. Such anisotropic growth

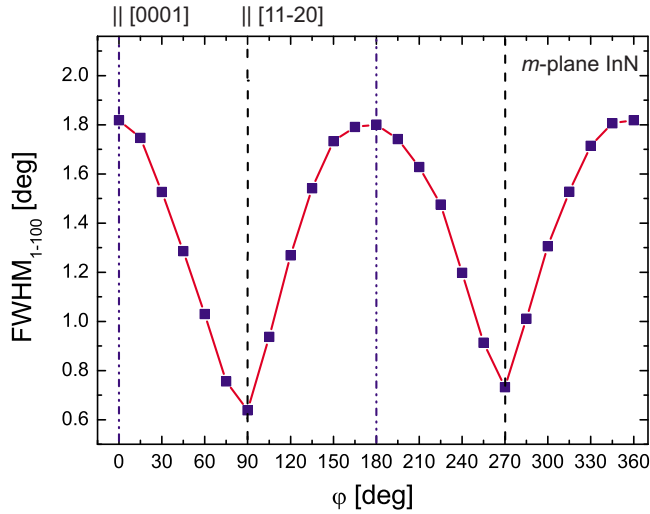


FIG. 7. (Color online) FWHM of the on-axis $(1\bar{1}00)$ RC for the m -plane InN film.

rates in the two orthogonal in-plane directions has been previously suggested for a -plane GaN films grown by MOVPE on r -plane sapphire.^{13,40}

In addition, Frank–Shockley-type partial dislocations could also contribute to the observed RC broadening. These dislocations bond the BPSFs and are expected to have anisotropic strain fields that will influence accordingly the RC broadening. Frank–Shockley-type partial dislocations have been previously suggested to contribute to the anisotropic broadening of the $(h\bar{h}2\bar{h}0)$ RC of HVPE a -plane GaN films.¹⁵

The values of the LCLs evaluated from the $(h\bar{h}00)$ Williamson–Hall plots (Table II) are larger and the respective BPSF densities (Table II) lower for the a -plane InN films grown at higher temperatures (films A1 and A3). The fact that the $(3\bar{3}00)$ RC FWHMs of the three a -plane InN films differ significantly (Fig. 6) indicates the presence of different densities of defects other than BPSFs. The latter suggests that the BPSF densities in our films might be overestimated to a different degree as they are presumed to be the major defect leading to the $(h\bar{h}00)_{h=1,2}$ RC broadening. However, other factors such as surface roughness may also contribute to the observed difference in the $(3\bar{3}00)$ RC widths. The divergence of the $(3\bar{3}00)$ RC FWHM with respect to the trend given by the $(1\bar{1}00)$ and $(2\bar{2}00)$ RCs (Fig. 6) increases with decreasing film surface roughness (Table II). Similar observation was reported for MOVPE a -plane GaN films and suggested to be due to the effect of strain relief associated with surface roughness.¹⁸ Given the possible overestimation of the BPSF density in our films, it is worth mentioning that the BPSF densities in films A1 and A3 are lower than the respective values for a -plane InN films grown on GaN substrates.²⁷ Note that in the latter the BPSF densities obtained from XRD have been confirmed by TEM.²⁷

2. m -plane InN

In contrast to the a -plane films, the on-axis RC FWHM of the m -plane InN film has a maximum at azimuth position

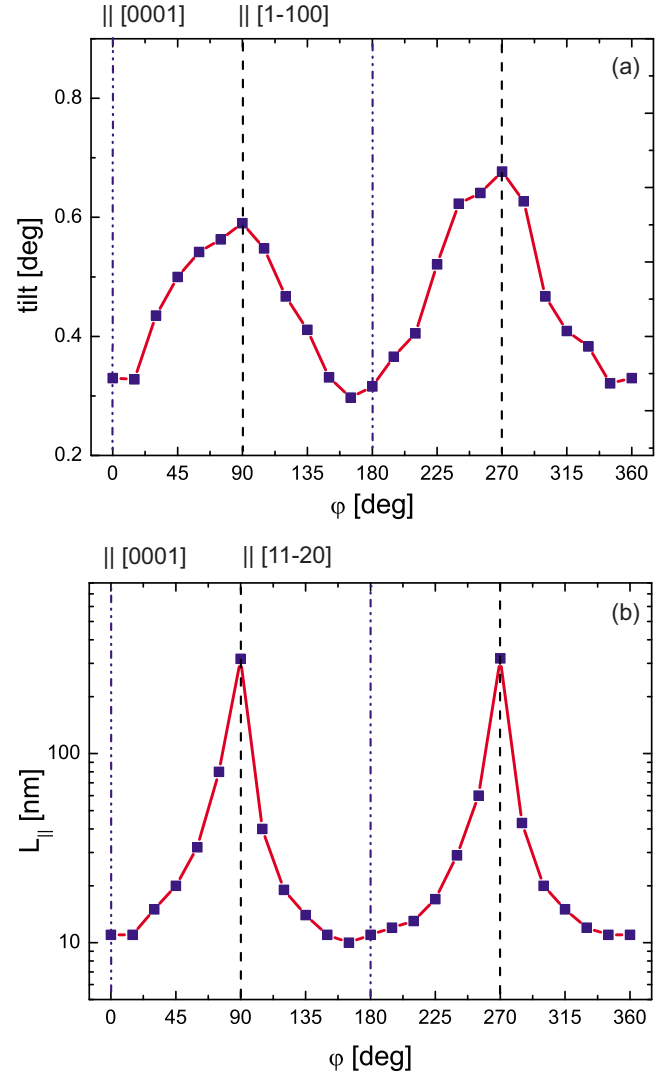


FIG. 8. (Color online) Azimuth dependencies of the tilt (a) and LCLs (b) for the m -plane InN film.

parallel to the InN $[0001]$ and a minimum for the perpendicular direction (see Fig. 7 and Table II). Such an anisotropic dependence of the $(1\bar{1}00)$ RC width was also reported for m -plane InN films grown by MBE on free-standing GaN (Ref. 26) and for m -plane GaN films grown by MBE, MOVPE, and HVPE on m -plane SiC.¹⁷ It is interesting to mention that the RC broadening in the InN $[0001]$ direction of our m -plane film (Table II) is slightly lower than the respective value of 1.86° for the m -plane InN grown at optimal conditions (lowest density of BPSFs) on GaN free-standing substrate.²⁶ Note that no special nucleation scheme was employed for the growth of our m -plane InN film (Table I) and a proper initial growth process, such as two-step growth, will likely improve the crystal quality³⁰ and further reduce the RC FWHM.

The mosaic tilt has a minimum for the InN $[0001]$ direction and the LCLs have maximum for the InN $[11\bar{2}0]$ direction (Fig. 8). This indicates that the contribution of the LCLs to the RC broadening is dominant in this case. This result is different from the structural anisotropy observed for the a -plane InN films with predominant RC broadening due to

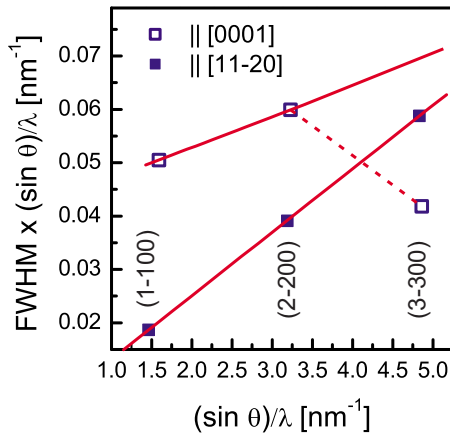


FIG. 9. (Color online) Williamson–Hall plots of the $(h\bar{h}00)$ RCs for the m -plane InN film at azimuth positions parallel and perpendicular to the InN [0001].

mosaic tilt, where the rotational disorder has minimum and the LCLs have maximum for the same azimuth positions parallel to the InN [0001].

The $(1\bar{1}00)$ and $(2\bar{2}00)$ RC FWHMs are larger for the InN [0001] azimuth position (Fig. 9 and Table II) implying significant contribution of BPSFs to the RC broadenings. On the other hand, the $(3\bar{3}00)$ RC, which is insensitive to the presence of BPSFs, is narrower for the InN [0001] direction (Fig. 9). More specifically, the $(3\bar{3}00)$ RC FWHMs are 0.70°C and 0.40°C for InN [11 $\bar{2}0$] and [0001], respectively. This observation indicates that defects different from BPSFs contribute considerably to the RC broadening and are responsible for the $(3\bar{3}00)$ RC anisotropy. Indeed the observed $(3\bar{3}00)$ RC anisotropy could be correlated with the mosaic tilt. Previously, a larger broadening of the $(3\bar{3}00)$ RC broadening in the InN [0001] direction was reported for m -plane InN films grown by MBE on GaN free-standing substrates,²⁶ and for m -plane GaN films grown by HVPE on SiC,¹⁷ while for MOVPE and MBE m -plane GaN on SiC the $(3\bar{3}00)$ RCs were found to have similar FWHMs for the two orthogonal in-plane directions.¹⁷ In all these cases the $(3\bar{3}00)$ RC FWHMs correlate with the mosaic tilt. Furthermore, the large anisotropy in the $(3\bar{3}00)$ RC broadening for the two orthogonal directions of m -plane InN films grown by MBE on GaN free-standing substrates was related to a deterioration of overall crystal quality with increasing growth temperature (which resulted in thermal decomposition).²⁶ Although our growth temperature is relatively high (Table I), the very narrow $(3\bar{3}00)$ RCs (0.70° and 0.40° for InN [11 $\bar{2}0$] and [0001] directions, respectively) and the lack of any In droplets at the surface of our m -plane InN film exclude thermal decomposition as a possible factor affecting the RC anisotropy in our case.

3. Semipolar $(10\bar{1}1)$ InN

The PF measurements around the InN $(10\bar{1}1)$ reflection (Fig. 10) of the semipolar InN film reveals the presence of two domains rotated with respect to each other by $\sim 93^\circ$.

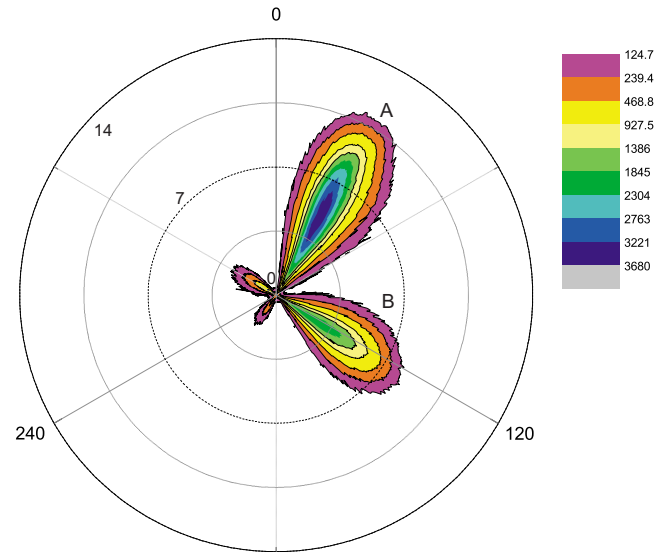


FIG. 10. (Color online) PF in stereographic projection of the $(10\bar{1}1)$ reflection for the semipolar InN film.

This result is in agreement with the AFM observations of the two rectangular domains nearly perpendicular to each other [Fig. 2(e)]. Domain A is tilted with respect to the surface normal by 4.8° while domain B is tilted by 2.7° . The difference in the inclination of the two domains accounts for the slight deviation from 90° in their azimuth orientation. A comparison between the integral intensities of the $(10\bar{1}1)$ reflection (Fig. 10) indicates that the volume fraction of domain A is about two times larger than that one of domain B. The presence of two domains in the semipolar films is in contrast to the results for the a -plane films, where only one domain was detected. The latter was also confirmed by PF measurements around the InN $(11\bar{2}0)$ reflection (not shown here).

The semipolar and a -plane InN films are both grown on r -plane sapphire. However, the nucleation stage in the two cases is different, which could explain the observed different structural anisotropy. The a -plane films are grown using nitridation of the substrate (Table I) leading to the formation of zinc-blende AlN (Ref. 29) or amorphous AlO_xN_y .²⁸ These nucleation layers serve as templates for the growth of the nonpolar wurtzite film with unique epitaxial relationship with respect to the substrate.²¹ On the other hand, the semipolar film is grown directly on the substrate without any nitridation (Table I). It has been previously shown that direct growth of InN on r -plane sapphire results in the nucleation of zinc-blende InN due to the much lower lattice mismatch compared to the wurtzite InN.⁴¹ Indeed, the HRTEM images taken from the interface region of our semipolar InN film revealed the presence of zinc-blende InN with (002) orientation at the interface with the substrate (Fig. 11). This result is further confirmed by selective area electron diffraction patterns (not shown). The zinc-blende phase of group-III nitrides is metastable and the wurtzite crystal structure is easily formed as a result of faulting of the stacking sequence. We observed that the SFs related to the wurtzite phase are formed in our semipolar InN film already in the interface region (Fig. 11). The wurtzite InN (0001) planes are stacked

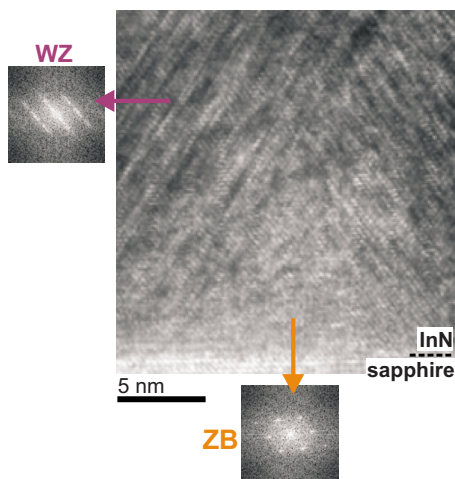


FIG. 11. (Color online) HRTEM image taken from the interface region of the semipolar InN film. The fast Fourier transformations from the two distinct regions: ZB—containing zinc-blende InN and WZ—containing mixture of wurtzite and zinc-blende InN are also shown.

along the zinc-blende InN (111) planes. Once formed, these wurtzite crystallites are thermodynamically stable and cannot be eliminated. The resulting semipolar film has the $(10\bar{1}1)$ plane nearly parallel to the surface. The PF measurements indicate that the wurtzite (0001) planes formed on both A and B zinc-blende (111) planes, which are rotated by 90° with respect to each other. Note that the two (111) faces are crystallographically equivalent but differently terminated, which is expected to control the polarity of the wurtzite InN (0001) grown atop. That is, (0001) (In-polar) InN will grow on zinc-blende InN (111)A and $(000\bar{1})$ (N-polar) will grow on zinc-blende InN (111)B.⁴² The growth rate of the wurtzite In-polar plane may be expected to be greater than the growth rate of the N-polar counterpart in similarity to GaN.^{8,43} This can qualitatively explain the detected higher volume fraction of $(10\bar{1}1)$ A domain compared to $(10\bar{1}1)$ B domain (see Fig. 10). The reasons behind the different growth rates along the two polar directions in group-III nitride epitaxial layers are not well understood. According to density functional theory calculations the energetically favorable surface reconstructions of InN polar surfaces are cation stabilized independently on the III/V ratio.⁴⁴ If InN is growing with In polarity, the surface N atoms must be bound to one underlying atom, while for N-polarity the N atom must bound to three underlying In atoms. It is therefore reasonable to expect that the surface N atoms desorb more easily from the In-polarity front than from the N-counterpart. Due to the enhanced desorption of the surface N the effective V/III ratio is different at the two fronts, which will affect the growth kinetics. Furthermore, N-polar InN surfaces typically have rough morphologies, which are inferior to the smooth In-polar surfaces in terms of InN crystal growth.

Previously, the formation of only one wurtzite $(10\bar{1}1)$ domain (near the film surface) has been reported for InN with predominant zinc-blende structure.⁴¹ Note that the ratio of wurtzite-to-zinc-blende-phase formation in the MBE growth of group-III nitrides strongly depends on the growth conditions,⁴⁵ which can explain the different results.

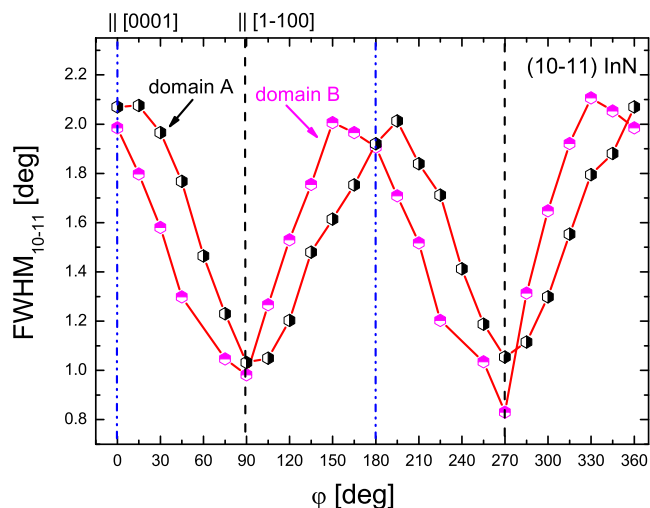


FIG. 12. (Color online) FWHM of the on-axis $(10\bar{1}1)$ RC for the semipolar InN film.

Both domains in the semipolar InN film show similar azimuth dependence of the $(10\bar{1}1)$ RC FWHM with maxima for the respective $[0001]$ directions and minima for the perpendicular directions (Fig. 12). The slight disturbance from the ideal “W”-shape at some azimuth positions could be related to the fact that the RCs of the two domains overlap in these cases and their FWHM are less accurately determined. The degree of anisotropy for the two domains is very similar being slightly higher than 1° . This implies that the mosaic tilt, being different for the two domains, could not be the determining factor responsible for the RC broadening. Further confirmation comes from the on-axis Williamson–Hall plot analysis. The obtained tilts have minima for the $[0001]$ and maxima for the perpendicular direction (Table II), which clearly does not follow the RC anisotropy with maxima for $[0001]$ and minima for the perpendicular direction (Fig. 12). The $(h0\bar{h}0)$ Williamson–Hall plot analysis further shows that the LCLs in $[0001]$ direction of domain A are significantly larger than those of domain B. The AFM results (Fig. 2) complemented with secondary electron microscopy show that the geometrical size of the crystallites could not be the limiting factor for the observed large on-axis RC broadening. Grain boundaries, planar, and extended defects are the most likely candidates.

The x-ray rocking directions for the $(h\bar{h}00)_{h=1,2}$ reflections of the semipolar film include angles of 90° with the InN $[0001]$ direction. Therefore, according to the visibility criteria these reflections will not be broadened by BPSFs.^{17,18} Indeed, the FWHM of the $(h\bar{h}00)$ RC decreases only very little with increasing the reflection order for both domains. The $(h\bar{h}00)$ Williamson–Hall plots further show that in contrast to the a -plane InN films, the $(3\bar{3}00)$ RC of the semipolar film lies almost perfectly on the trend set by the $(1\bar{1}00)$ and $(2\bar{2}00)$ reflections (Fig. 13). It should be noted that substantial part of the growth of the semipolar film might proceed along the $[0001]$ direction for domain A, which will lead to great reduction in BPSF formation.⁸ However, additional structural analysis is required to confirm this speculation.

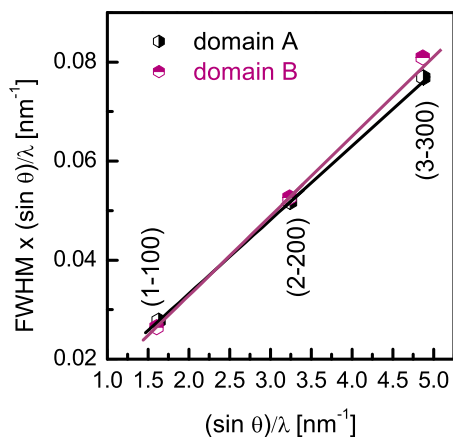


FIG. 13. (Color online) Williamson–Hall plots of the $(h\bar{h}00)$ RCs for the $(10\bar{1}0)$ InN film at azimuth positions parallel to the InN $[0001]$ direction for the respective domain.

IV. CONCLUSIONS

The structural anisotropy of MBE a -plane and $(10\bar{1}1)$ InN films on r -plane sapphire and m -plane InN film on (100) γ -LiAlO₂ have been studied. We found that all a -plane films show a characteristic on-axis RC anisotropy with minima for the $[0001]$ direction and maxima for the perpendicular direction, independently on the nucleation scheme and growth conditions. The degree of the structural anisotropy and its magnitude can be minimized by combing higher nitridation temperature and higher growth temperature in order to reduce the tilt and enhance the LCLs. Furthermore, we discussed the different factors affecting the RC broadening for the a -plane InN films and suggested that surface roughness and film curvature could not be responsible for the observed RC anisotropy. On the other hand, the geometrical size of the crystallites, governed by the anisotropic growth rate in $[0001]$ and $[11\bar{2}0]$ directions, and the Frank–Shokley-type partial dislocations seem to be good candidates to explain this RC anisotropic behavior. The m -plane and semipolar InN films show on-axis RC anisotropy with maxima for the $[0001]$ direction and minima for the perpendicular direction. We concluded that the LCL is the dominant factor causing the RC broadening and anisotropy in the m -plane film, which is mainly determined by the BPSF and extended defect densities, while the tilt plays a minor role. In contrast to the nonpolar films, the semipolar InN is found to contain two domains, A and B, rotated with respect to each other by $\sim 90^\circ$, and which nucleate on zinc-blende InN(111)A and (111)B faces, respectively. The much larger volume fraction of domain A compared to domain B is suggested to be a consequence of their different polarity: In (0001) -polarity for domain A and $N(000\bar{1})$ for domain B. It is worth noting that the BPSF densities in the nonpolar a - and m -InN films are lower than the respective values for films grown on GaN free-standing substrates.²⁶ Our results suggest that heteroepitaxy of nonpolar InN on sapphire and γ -LiAlO₂ could provide a less expensive alternative to native substrates for InN-based device heterostructures.

ACKNOWLEDGMENTS

This work is financially supported by FCT Portugal under Contract No. PTDC/FIS/100448/2008 and program Ciênciã 2007. We acknowledge support from the Swedish Research Council (VR) under Grant No. 2005-5054.

- ¹P. Waltereit, O. Brandt, A. Trampert, H. Grahn, J. Menniger, M. Ramsteiner, M. Reiche, and K. H. Ploog, *Nature (London)* **406**, 865 (2000).
- ²A. E. Romanov, T. J. Baker, S. Nakamura, and J. S. Speck, *J. Appl. Phys.* **100**, 023522 (2006).
- ³M. Craven, S. Lim, F. Wu, J. S. Speck, and S. P. DenBaars, *Appl. Phys. Lett.* **81**, 469 (2002).
- ⁴N. Onojima, J. Suda, T. Kimoto, and H. Matsunami, *Appl. Phys. Lett.* **83**, 5208 (2003).
- ⁵R. Armitage, M. Horita, J. Suda, and T. Kimoto, *J. Appl. Phys.* **101**, 033534 (2007).
- ⁶K. Okamoto, H. Ohta, D. Nakagawa, M. Sonobe, and J. Ichihara, *Jpn. J. Appl. Phys., Part 2* **45**, L1197 (2006).
- ⁷H. Yamada, K. Iso, M. Saito, H. Hirasawa, N. Fellows, H. Masui, K. Fujito, J. S. Speck, S. P. DenBaars, and S. Nakamura, *Phys. Status Solidi (RRL)* **2**, 89 (2008).
- ⁸T. Gühne, Z. Bougrioua, P. Venéguès, M. Leroux, and M. Albrecht, *J. Appl. Phys.* **101**, 113101 (2007).
- ⁹C. F. Johnston, M. A. Moram, M. J. Kappers, and C. J. Humphreys, *Appl. Phys. Lett.* **94**, 161109 (2009).
- ¹⁰G. T. Chen, S. P. Chang, J. I. Chui, and M. N. Chang, *Appl. Phys. Lett.* **92**, 241904 (2008).
- ¹¹H. Sato, R. B. Chung, H. Hirasawa, N. Fellows, H. Massui, F. Wu, M. Saito, K. Fujito, J. S. Speck, S. P. DenBaars, and S. Nakamura, *Appl. Phys. Lett.* **92**, 221110 (2008).
- ¹²H. Asamizu, M. Saito, K. Fujito, J. S. Speck, S. P. DenBaars, and S. Nakamura, *Appl. Phys. Express* **2**, 021002 (2009).
- ¹³H. Wang, C. Chen, Z. Gong, J. Zhang, M. Gaevski, M. Su, J. Yang, and M. A. Khan, *Appl. Phys. Lett.* **84**, 499 (2004).
- ¹⁴T. Paskova, V. Darakchieva, P. Paskov, J. Birch, E. Valcheva, P. O. A. Persson, B. Arnaudov, S. Tungasmita, and B. Monemar, *J. Cryst. Growth* **281**, 55 (2005).
- ¹⁵T. Paskova, R. Kroeger, S. Figge, D. Hommel, V. Darakchieva, B. Monemar, E. Preble, A. Hanser, N. M. Williams, and M. Tutor, *Appl. Phys. Lett.* **89**, 051914 (2006).
- ¹⁶C. Roder, S. Einfeldt, S. Figge, T. Paskova, D. Hommel, P. P. Paskov, B. Monemar, U. Behn, B. A. Haskell, P. T. Fini, and S. Nakamura, *J. Appl. Phys.* **100**, 103511 (2006).
- ¹⁷M. B. McLaurin, A. Hirai, E. Young, F. Wu, and J. S. Speck, *Jpn. J. Appl. Phys.* **47**, 5429 (2008).
- ¹⁸M. A. Moram, C. F. Johnston, J. L. Hollander, M. J. Kappers, and C. J. Humphreys, *J. Appl. Phys.* **105**, 113501 (2009).
- ¹⁹M. A. Moram, C. F. Johnston, M. J. Kappers, and C. J. Humphreys, *J. Phys. D: Appl. Phys.* **42**, 135407 (2009).
- ²⁰Q. Sun, B. Leung, C. D. Yerino, Y. Zang, and J. Han, *Appl. Phys. Lett.* **95**, 231904 (2009).
- ²¹V. Darakchieva, T. Paskova, M. Schubert, H. Arwin, P. P. Paskov, B. Monemar, D. Hommel, M. Heuken, J. Off, F. Scholz, B. Haskell, P. Fini, J. Speck, and S. Nakamura, *Phys. Rev. B* **75**, 195217 (2007).
- ²²S. Ghosh, P. Waltereit, O. Brandt, H. T. Grahn, and K. H. Ploog, *Phys. Rev. B* **65**, 075202 (2002).
- ²³T. Flissikowski, O. Brandt, P. Misra, and H. T. Grahn, *J. Appl. Phys.* **104**, 063507 (2008).
- ²⁴A. O. Ajagunna, E. Iliopoulos, G. Tsiakatouras, K. Tsagaraki, M. Androuridaki, and A. Georgakilas, *J. Appl. Phys.* **107**, 024506 (2010).
- ²⁵C. L. Hsiao, J. T. Chen, H. C. Hsu, Y. C. Liao, P. H. Tseng, Y. T. Chen, Z. C. Feng, L. W. Tu, M. M. C. Chou, L. C. Chen, and K. H. Chen, *J. Appl. Phys.* **107**, 073502 (2010).
- ²⁶G. Koblmüller, A. Hirai, F. Wu, C. S. Gallinat, G. D. Metcalfe, and J. S. Speck, *Appl. Phys. Lett.* **93**, 171902 (2008).
- ²⁷G. Koblmüller, G. D. Metcalfe, M. Wraback, F. Wu, C. S. Gallinat, and J. S. Speck, *Appl. Phys. Lett.* **94**, 091905 (2009).
- ²⁸C. L. Hsiao, T. W. Liu, C. T. Wu, H. C. Hsu, G. M. Hsu, L. C. Chen, W. Y. Shiao, C. C. Yang, A. Gällström, P.-O. Holtz, C. C. Chen, and K. H. Chen, *Appl. Phys. Lett.* **92**, 111914 (2008).
- ²⁹Y. Kumagai, A. Tsuyuguchi, H. Naoki, T. Araki, H. Na, and Y. Nanishi,

- Phys. Status Solidi B* **243**, 1468 (2006).
- ³⁰Y. Nanishi, T. Araki, and T. Yamaguchi, in *Indium Nitride and Related Alloys*, edited by T. D. Veal, C. F. McConville, and W. J. Schaff (CRC, New York, 2009), p. 28.
- ³¹V. Darakchieva, M. Schubert, T. Hofmann, B. Monemar, C. L. Hsiao, T. W. Liu, L. C. Chen, W. J. Schaff, Y. Takagi, and Y. Nanishi, *Appl. Phys. Lett.* **95**, 202103 (2009).
- ³²H. Lu, W. J. Schaff, L. F. Eastmann, J. Wu, W. Walukiewicz, V. Cimalla, and O. Ambacher, *Appl. Phys. Lett.* **83**, 1136 (2003).
- ³³T. Paskova, *Phys. Status Solidi B* **245**, 1011 (2008).
- ³⁴Y. J. Sun, O. Brandt, and K. H. Ploog, *J. Vac. Sci. Technol. B* **21**, 1350 (2003).
- ³⁵J. Smalc-Koziorowska, G. P. Dimitrakopoulos, S.-L. Sahota, G. Tsiakatouras, A. Georgakilas, and P. Komninou, *Appl. Phys. Lett.* **93**, 021910 (2008).
- ³⁶T. Metzger, R. Höppler, E. Born, O. Ambacher, M. Stuzmann, R. Stömmer, M. Schuster, H. Göbel, S. Christiansen, M. Albrecht, and H. P. Strunk, *Philos. Mag. A* **77**, 1013 (1998).
- ³⁷R. Chierchia, T. Böttcher, H. Heinke, S. Einfeldt, S. Figge, and D. Hommel, *J. Appl. Phys.* **93**, 8918 (2003).
- ³⁸V. Darakchieva, T. Paskova, P. Paskov, B. Monemar, N. Ashkenov, and M. Schubert, *J. Appl. Phys.* **97**, 013517 (2005).
- ³⁹T. Paskova, V. Darakchieva, E. Valcheva, P. Paskov, I. G. Ivanov, B. Monemar, T. Böttcher, C. Roder, and D. Hommel, *J. Electron. Mater.* **33**, 389 (2004).
- ⁴⁰X. Ni, Y. Fu, Y. T. Moon, N. Biyikli, and H. Morkoç, *J. Cryst. Growth* **290**, 166 (2006).
- ⁴¹V. Cimalla, J. Pezoldt, G. Ecke, R. Kosiba, O. Ambacher, L. Spieß, G. Teichert, H. Lu, and W. J. Schaff, *Appl. Phys. Lett.* **83**, 3468 (2003).
- ⁴²A. Koukitu, Y. Kumagai, and H. Seki, in *Nitrides as seen by the Technology*, edited by T. Paskova and B. Monemar (Research Signpost, Trivandrum, India, 2002).
- ⁴³F. Wu, M. D. Craven, S. H. Lim, and J. S. Speck, *J. Appl. Phys.* **94**, 942 (2003).
- ⁴⁴D. Segev and C. G. V. de Walle, *Surf. Sci.* **601**, L15 (2007).
- ⁴⁵B. Daudin, G. Feuillet, Y. Samson, F. Widmann, A. Philippe, C. Bru-Chervallier, G. Gillot, E. Bustarret, G. Bentoumi, and A. Deneuveille, *J. Appl. Phys.* **84**, 2295 (1998).